Impact of tropical cyclones on the ocean heat budget in the Bay of Bengal during 1999: 2. Processes and interpretations

Jih-Wang Wang,[1] Weiqing Han,[1] and Ryan L. Sriver[2]

Received 18 July 2012; accepted 8 August 2012; published 18 September 2012.

[1] The impacts of two consecutive, strong tropical cyclones (TCs) from October–November in 1999 on the Bay of Bengal (BoB) heat budget are examined using the Hybrid Coordinate Ocean Model. The model uses atmospheric conditions from reanalysis, reconstructed TC winds, and satellite-observed winds and precipitation. We conduct a series of diagnostic experiments to isolate the model's response to the individual TC-associated forcings. During the TCs, the BoB ocean heat content (OHC) is reduced, primarily due to TC-wind induced southward ocean heat transport (OHT) and a reduction in surface downward radiation due to increased cloudiness. BoB OHC is largely restored in the following months via enhanced surface heat fluxes, associated with cold wake restoration, and positive northward OHT. The TCs' downward heat pumping effect is estimated to be $\sim 1.74 \times 10^{18}$ J near the end of February 2000, which is less than estimates using previously published methods based on surface observations. The relatively weak heat pumping results from freshwater input by intense monsoon rainfall and river discharge in the BoB, which stabilizes stratification, forms a barrier layer, and generates temperature inversions during seasonal surface cooling. As a result, early stage TC winds entrain the warm barrier layer water and enhance enthalpy loss in the southeastern Bay, while mature stage TC winds erode the barrier layer, decrease SST through upwelling and entrainment of deeper cold water and reduce enthalpy loss in the northwestern Bay. Our findings suggest TC winds may significantly alter the interseasonal BoB heat budget through OHT and surface heat fluxes.

Citation: Wang, J.-W., W. Han, and R. L. Sriver (2012), Impact of tropical cyclones on the ocean heat budget in the Bay of Bengal during 1999: 2. Processes and interpretations, *J. Geophys. Res.*, *117*, C09021, doi:10.1029/2012JC008373.

1. Introduction

[2] Previous studies suggest that downward ocean heat pumping (DOHP) by tropical cyclones (TCs), which measures the amount of heat that is pumped down from the mixed layer (ML) into the thermocline due to TC winds-induced turbulent mixing process, may be responsible for substantial amount of oceanic meridional heat transport [e.g., *Emanuel*, 2001; *Wang et al.*, 2012, hereinafter referred to as part 1]. Several observational [*Sriver and Huber*, 2007; *Sriver et al.*, 2008; *Jansen et al.*, 2010] and modeling [e.g., *Jansen and Ferrari*, 2009; *Sriver and Huber*, 2010; *Sriver et al.*, 2010; *Fedorov et al.*, 2010; *Manucharyan et al.*, 2011] studies have been conducted to investigate the DOHP effect and the impacts of TCs on global ocean heat budget and transport, and yielded mixed results. It appears there are several factors that modulate the oceanic response to TCs, such as regional differences in the background state, timing of the TC occurrence, and size, intensity and translation speed of the TC event [e.g., *Sriver and Huber*, 2010; *Sriver et al.*, 2010].

[3] Most of the previous studies that investigated the impacts of TCs on the upper ocean heat budget focused on the effects of winds [e.g., *Jacob et al.*, 2000; *Emanuel*, 2001]; however, other processes may also be important. For example, a recent modeling study by *Hu and Meehl* [2009] suggested that the effect of hurricane rainfall could counteract the effect of hurricane winds. While the hurricane winds enhance northward heat transport of the Atlantic meridional overturning circulation, the precipitation reduces it through meridional redistribution of freshwater originating in the tropics. Thus, the overall effect on ocean heat transport (OHT) depends on the relative magnitude of these two competing processes. *Jansen et al.* [2010], on the other hand, suggested that the TC effects on DOHP may be greatly reduced due to the seasonal ML deepening and ocean heat release back to the atmosphere. While these recent studies

[1]Department of Atmospheric and Oceanic Sciences, University of Colorado Boulder, Boulder, Colorado, USA.
[2]Department of Atmospheric Sciences, University of Illinois at Urbana-Champaign, Urbana, Illinois, USA.

Corresponding author: J.-W. Wang, Department of Atmospheric and Oceanic Sciences, University of Colorado Boulder, 311 UCB, Boulder, CO 80309, USA. (jihwang@colorado.edu)

0148-0227/12/2012JC008373

have broken important new ground related to the relationship between TCs and climate lined to upper ocean processes and air-sea interactions, the use of high-resolution ocean models could provide a useful tool for developing a better understanding and quantification of the processes associated with TC-climate impacts via strong winds, precipitation, surface turbulent heat fluxes, and shortwave and longwave radiation.

[4] The goal of this study is to understand how the upper ocean in the Bay of Bengal (BoB) responded to two consecutive, strong TCs – 04B (10/15–10/19) and 05B (10/25–11/3) that landed at Orissa in 1999 (hereafter, TC1 and TC2, respectively), with special emphasis on the upper ocean heat budget, including DOHP and OHT. We conduct a series of experiments using an Ocean General Circulation Model (OGCM) – the HYbrid Coordinate Ocean Model (HYCOM), to assess the processes by which the two TCs caused the upper ocean heat change. In this paper, we quantify the DOHP effect from the perspective of air-sea heat exchange, by estimating the difference of ocean surface heat gain between the model simulations with and without TCs, which avoids the assumption of negligible surface heat flux during the TCs and sea surface temperature (SST) cooling induced entirely by vertical mixing [e.g., *Emanuel*, 2001; *Sriver and Huber*, 2007; *Sriver et al.*, 2008]. The rest of the paper is organized as follows. Section 2 describes the experiment design and the method of removing TC signals from the forcing fields. Section 3 reports our results, and section 4 provides summary and conclusions.

2. TC Signal Removal and Experiment Design

[5] In Part 1 [*Wang et al.*, 2012], we described the HYCOM configuration and its surface forcing fields, which are Cross-Calibrated MultiPlatform (CCMP) satellite winds, European Center for Medium-Range Weather Forecasts (ECMWF) Re-analysis Interim (ERAI) data, Tropical Rainfall Measuring Mission (TRMM) precipitation, and reconstructed TC winds. In this section, we demonstrate how to remove the TC signals from the forcing fields so that we can isolate their impacts by comparing HYCOM simulations with and without these signals.

2.1. TC Signal Removal

[6] In many existing studies (see part 1, section 1.1), the TC effect on ocean heat content (OHC) and SST is estimated by comparing the sea state before and after a TC event. The "before-vs.-after" method, however, is not able to isolate the processes through which TCs affect the ocean. For example, does the effect of TC rainfall counteract the effect of TC wind on OHT, as suggested by *Hu and Meehl* [2009]? Our OGCM experiments improve previous works by using a high-resolution ocean model capable of resolving the processes important for TC-induced changes in OHC and OHT on intraseasonal and seasonal timescales. This methodology is not restricted by previous assumptions, such as those related to post-storm SST recovery and assumed mixing depths.

[7] As discussed in part 1, HYCOM is initially spun up for 20 years using the ERAI 1989–2008 monthly climatological forcing fields, and then integrated forward in time for the period of 1989–2000 using the 6-hourly forcing fields for the Main Run (MR). An experimental run, named RcWIND, has also been performed using the reconstructed TC winds, in order to understand the effect of TC-associated strong winds, which are significantly underestimated by both CCMP and ERAI products. To quantify the 1999 TCs' effects, an additional suite of diagnostic experiments is performed by excluding the TC-associated forcing fields. We first filter out TC signals from the forcing fields (i.e., wind, precipitation, shortwave radiation, longwave radiation, air temperature, and air humidity) using a low-pass Lanczos digital filter [*Duchon*, 1979]. Based on the radii of 18-m/s (~35-kt) winds and translation speeds of the two TCs, we find that the changes in wind direction and strength associated with the storms have a period within 7.5 days over the ocean. We thus choose 8 days as the half power point cutoff period for the low-pass filtering to remove the TCs. The filtered forcing fields from 9/22 18Z to 11/25 12Z in 1999 are used to force HYCOM in the experimental runs. Linear ramping is used in time and space to ensure the smooth transition from the unfiltered to filtered fields. For space ramping, we define the ramping weight as

$$ramp_{space} = \begin{cases} 0 & \text{, if inside the BoB} \\ (x - x_{in})/(x_{out} - x_{in}) & \text{, if in the ramping area} \\ 1 & \text{, otherwise} \end{cases} \quad (1)$$

x_{out} is the outer boundary of the ramping area, and x_{in} the inner boundary. In our study, the ramping area is set to 5 degrees. A similar concept is applied to time ramping, with the ramping time zone set to 4 days. The total ramping weight is

$$weigth = \left(1 - ramp_{space}\right) \times \left(1 - ramp_{time}\right) \quad (2)$$

[8] The surface wind speed (U) in the ramping area and period, for instance, is then defined as

$$U^{*} = weight \times U' + (1 - weight) \times U \quad (3)$$

[9] The filtering method is successful in removing the vortex wind structure (compare Figures 1a and 1b), although there is still minor vortex-like circulation near the TC center after the filtering, which can be largely attributed to the steering flow. The outer most 5-degree ramping area along the lateral boundaries has very little vortex-like circulation (not shown). Surface net solar radiation (SRnet) is treated differently from the other forcing fields to retain the diurnal cycle in solar radiation in the filtered time series. The regular 8-day low-pass filtering normally removes the diurnal cycle in solar radiation, which is *not* a property of a TC; therefore, the targeted time series for filtering should be the percentage of solar radiation that is deducted by the TC. We define ΔSRnet as the difference between SRnet and the maximum possible SRnet (MaxSRnet) at the time of the day during the filtering period. That is, MaxSRnet has four values, which correspond to the maximum possible SRnet at 00Z, 06Z, 12Z, and 18Z during the period of 9/22 18Z–11/25 12Z in 1999. The ratio of ΔSRnet to MaxSRnet is then filtered, similar to the other forcings. The filtered time series multiplied by MaxSRnet according to the time of the day forms the new SRnet time series that represents the surface net solar radiation without a TC. By doing this, the TC signal at diurnal frequency is still filtered, because the TC signal is reflected in the ratio of ΔSRnet to MaxSRnet; meanwhile,

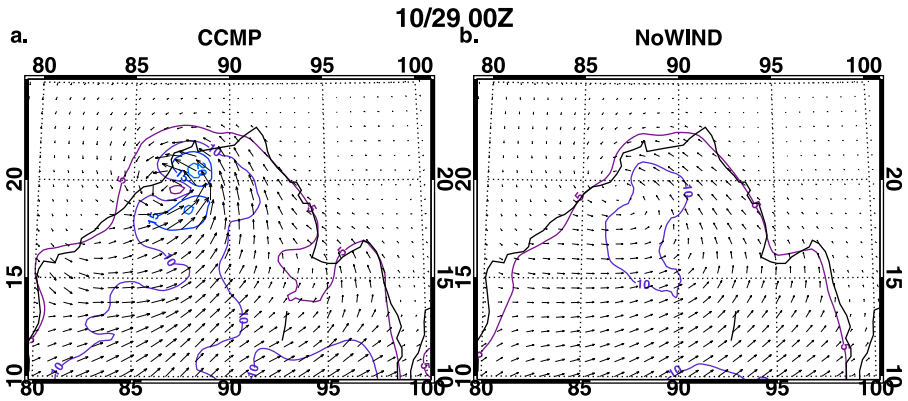

Figure 1. Wind speed (contours; 5 m/s interval) and wind velocity (arrows) for the products from (a) CCMP and (b) filtered CCMP.

the solar diurnal cycle is retained so as not to interfere with our analysis when isolating the effect of TC-associated radiation reduction.

2.2. Experiment Design

[10] A set of experiments (EXPs) is performed branching from the MR solution on 10/11 in 1999 by forcing HYCOM with the TC-removed forcing fields during the two TCs' periods (Table 1). The experimental run that uses the reconstructed TC winds from part 1 – RcWIND – is also included in our analysis. While the seven EXPs and MR have the same values before 10/11 in 1999, the differences between the MR and EXPs solutions afterwards provide quantitative estimates of the effects of TC-associated forcing fields.

[11] The model runs are divided into three groups, according to their purposes. Group A (MR and RcWIND) contains control runs and is used to compare with the observations (part 1) and other experiment results. Group B (NoWIND, RcWIND, NoRAIN, NoRAD and NoTC) is designed to examine the effects of wind, rain, radiation, and other forcings on surface heat flux and OHT. Group C (NoWSTR and RcWSTR) is specifically designed to investigate the effects of wind stress. Each of the EXPs has certain filtered or reconstructed forcing fields (see Table 1). In EXP NoWIND, NoRAIN, NoRAD, NoWSTR and NoTC, HYCOM is forced by 8-day low-pass filtered wind (wind stress and wind speed), filtered rain, filtered radiation, filtered wind stress, and the whole set of filtered surface forcings, respectively, during the 10/11 00Z-11/7 06Z period in 1999. All the surface forcings in the EXPS are the same as in the MR otherwise. Note that NoWIND and RcWIND represent the experiments in which HYCOM is forced by filtered wind fields and reconstructed wind fields, respectively, for TC1 and TC2.

3. Results

[12] In section 3.1, we examine the impacts of the two TCs on the BoB DOHP, OHT and the associated physical processes. In section 3.2, we compare the DOHP estimated from the existing methods and from HYCOM simulations for TC1 and TC2. Finally, in sections 3.3 and 3.4, we discuss the depth penetration of the two-TC effects and the effects on the BoB heat potential.

Table 1. The Suite of HYCOM Experiments Performed for Assessing the TCs' Impacts[a]

Group	Model Runs	Forcings	Space Ramping	Time Ramping	Study Purpose
A	MR	air temperature, radiative flux, and humidity from ERAI; wind from CCMP; rain rate from ERAI before 1998, from TRMM since 1998	None	None	Model/data comparison
A and B	RcWIND	wind speed and stress re-constructed for high wind period of TC1 and TC2	2 times of 35-kt radius	None	Model/data comparison and effect of wind
B	NoWIND	wind speed and stress filtered for TC1 and TC2	70°E–75°E, 105°E–110°E, 0°–5°N.	Before TC1 and after TC2	Wind processes (mixing, transport, fluxes, etc.)
B	NoRAIN	precipitation filtered for TC1 and TC2	70°E–75°E, 105°E–110°E, 0°–5°N	before and after TC2	Effect of rain
B	NoRAD	radiative fluxes filtered for TC1 and TC2	70°E–75°E, 105°E–110°E, 0°–5°N	before and after TC2	Effect of radiation
B	NoTC	all the forcings filtered for TC1 and TC2	70°E–75°E, 105°E–110°E, 0°–5°N	before and after TC2	Total TC effects
C	NoWSTR	wind stress filtered for TC1 and TC2	70°E–75°E, 105°E–110°E, 0°–5°N.	Before TC1 and after TC2	Wind processes (mixing, transport, etc.)
C	RcWSTR	wind stress re-constructed for high wind period of TC1 and TC2	2 times of 35-kt radius	None	Model comparison and effect of wind stress

[a]The abbreviation "WIND" stands for wind speed and wind stress, "RAIN" for rain rate, "RAD" for radiation, "WSTR" for wind stress, "WSPD" for wind speed, "No" for filtered, and "Rc" for reconstructed. See text for detailed description of each experiment.

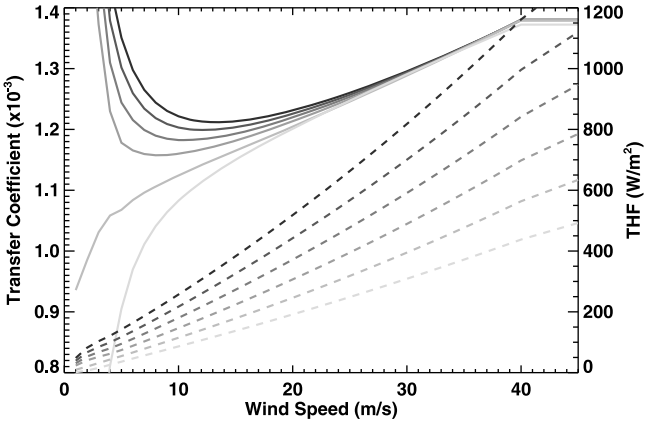

Figure 2. Transfer coefficients (solid) and THF (dashed) curves for SST being 4°C, 3°C, 2°C, 1°C, 0°C, and −1°C (from dark to light) warmer than the air temperature with wind speed from 5 m/s to 40 m/s and above, assuming 2 m air temperature as 26°C, relative humidity as 80% and pressure as 1013 mb. The curves are produced based on COARE 3.0 algorithm [*Fairall et al.*, 2003].

3.1. Impacts of TCs on the BoB Heat Balance

3.1.1. Processes That Affect the BoB OHC

[13] The OHC in our study is defined as OHC = mC_p (θ − 26), where m is seawater mass, Cp = 3990 J/K·kg specific heat, and (θ − 26) potential temperature relative to 26°C. The reference temperature, 26°C, is chosen so that the OHC quantity in the upper ocean can reflect TC heat potential [*Gray*, 1979]. The processes that can change the total (from surface to bottom) OHC in the BoB include surface turbulent heat flux (THF), which is sensible heat flux plus latent heat flux, surface radiative fluxes (shortwave + longwave fluxes), and horizontal heat transport and mixing. The surface net heat flux (NetHF) is the sum of THF and radiative fluxes (NetHF = THF + radiative flux).

[14] The sensible heat flux is parameterized in HYCOM with the equation:

$$H = C_{p_{air}}(0.9554E_x)(T_s - T_a), \tag{4}$$

where C_{Pair} is specific heat of the air, T_s is SST, T_a is temperature in the atmospheric boundary layer, and E_x is an exchange coefficient. A similar equation is used for surface latent heat flux:

$$\varepsilon = E_x L(H_u - E_v), \tag{5}$$

where L is latent heat of vaporization, H_u is specific humidity, and E_v is 0.97 × saturated humidity with respect to SST. Exchange coefficient $E_x = \rho_a C_T W$, where ρ_a is air density, C_T is heat transfer coefficient, and W is wind speed. C_T follows the Coupled Ocean-Atmosphere Response Experiment (COARE 3.0) algorithm [*Fairall et al.*, 2003], which is a complex function of wind speed and atmospheric stability and increases with wind speed up to 40 m/s. Thus, E_x and THF both increase with wind speed, unless the temperature and humidity gradients between the sea and air are zero.

[15] Strong winds associated with the TCs can affect THF and thus OHC. Figure 2 shows the THF under both unstable (SST is 0.75°C warmer than the 2 m air temperature) and stable (SST is 0.75°C colder than the 2 m air temperature) conditions [*Fairall et al.*, 2003] for a wide range of wind speed. While wind speed appears to be the strongest factor for changing THF magnitude, lower SST can also significantly reduce the THF to the atmosphere.

[16] TC-associated winds can also induce upper-ocean mixing and DOHP, potentially altering ocean circulation and affecting OHT. Mixing in the ocean interior in HYCOM is represented by the K-Profile Parameterization (KPP) scheme. Mixing is triggered when gradient Richardson number $Ri_g < 0.7$, which is defined as

$$Ri_g = \frac{N^2}{\left(\frac{\partial \bar{u}}{\partial z}\right)^2 + \left(\frac{\partial \bar{v}}{\partial z}\right)^2},$$

where N is Brunt-Väisälä frequency. Mixing in the surface boundary layer is active from the surface to the depth where bulk Richardson number $Ri_b < 0.15$, which is defined as

$$Ri_b = \frac{(B_r - B)d}{(\bar{V}_r - \bar{V})^2 + V_t^2},$$

where B is buoyancy, d is the depth of the boundary layer, the subscript r denotes reference values, and the two terms in the denominator represent the influence of resolved vertical shear and unresolved turbulent velocity shear, respectively. For the upper Indian Ocean, the velocities that appear in the denominators of both the Richardson numbers are mostly driven by winds. In HYCOM, there is an option of choosing wind speed or wind stress to determine frictional velocity (u*), which in turn determines unresolved turbulent velocity shear. We choose the latter, and hence our mixing in KPP scheme mainly depends on wind stress. Strong wind stress transfers momentum to the ocean surface, changes current velocities, and thus may induce vertical shear instability and mixing in the upper ocean.

3.1.2. BoB OHC Budget: Relative Importance of Wind, Precipitation and Radiation Forcing

3.1.2.1. Seasonal Cycle of BoB OHC

[17] Before we analyze the TC effects on the BoB OHC budget, it is essential to examine the seasonal cycle of the BoB OHC as the background variability. The total OHC of the BoB from the MR experiences relatively small perturbation (<150 × 10^{18} J) from mid-October to early November in 1999 that covers the durations of TC1 and TC2, and a major increase (>1,100 × 10^{18} J) from early November to late December after the TCs (Figure 3a). The total OHC stays high during January and February of year 2000. The NetHF accumulation (i.e., integration over time) north of 10°N acts to reduce the OHC rather than increase it, as shown by the quick decrease of NetHF from mid-November to mid-January. This is because the warm SST and cool air temperature associated with the winter monsoon cause turbulent heat loss, which exceeds the declining net radiative flux (not shown), resulting in negative NetHF. The OHC increase, therefore, results primarily from the seasonal, northward meridional OHT accumulation across 10°N integrated from the surface to bottom, a result that is consistent with previous studies [*Wacongne and Pacanowski*, 1996; *Lee and Marotzke*, 1998; *Webster et al.*, 2002]. The

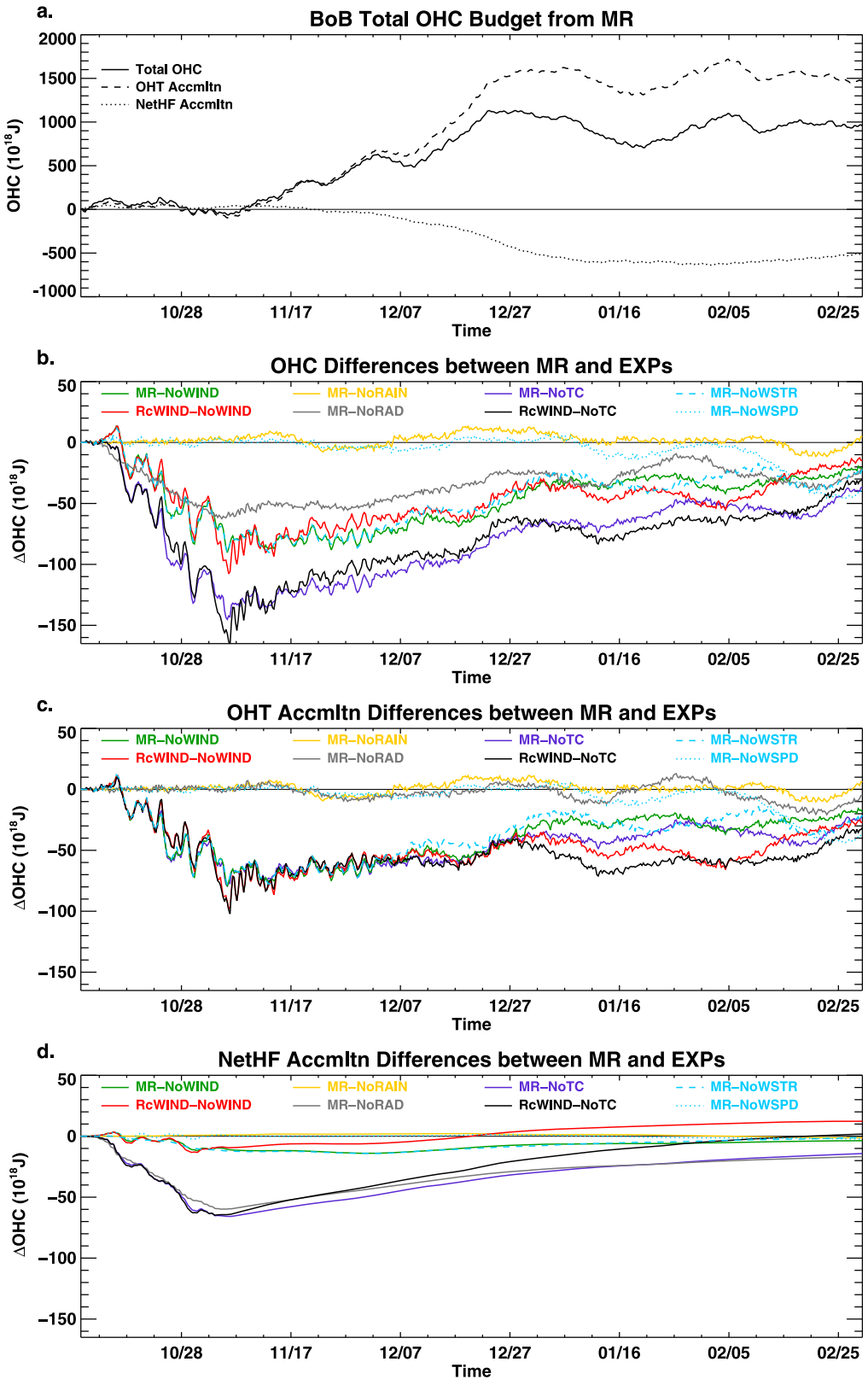

Figure 3. (a) Temporal variations of the BoB OHC, which is the OHC integrated over the region north of 10°N for the entire water column, together with the temporarily accumulated NetHF and meridional OHT from the MR. (b) The differences of OHC between the MR and EXPs for the BoB. (c) Same as Figure 3b but for the differences of meridional OHT accumulations. (d) Same as Figure 3b but for the differences of NetHF accumulations. OHT is defined as the meridional heat transport across 10°N into the BoB, and is calculated as the residual of OHC change subtracting NetHF accumulation.

meridional OHT accumulation across 10°N rapidly increases from 0 to ~1,600 × 10^{18} J from early November to late December in 1999.

3.1.2.2. TC-Induced OHC Change

[18] The total OHC differences between the MR and the series of EXP runs isolate the impacts of wind, precipitation, radiation and other forcings associated with TC1 and TC2 on OHC variations (Figure 3b). The TCs dramatically reduce the BoB OHC from 10/15–11/5 when they pass the BoB, and the BoB OHC slowly recovers afterwards (MR–NoTC and RcWIND–NoTC; purple and black curves). The reduction of the OHC results primarily from TC-associated wind (MR-NoWIND and RcWIND-NoWIND; green and red curves) and radiation (MR-NoRAD; gray curve). The effect of precipitation (MR-NoRAIN; yellow curve) is small, compared to wind and radiation. The total effects of TC1 + TC2 are comparable to OHC seasonal variations before mid-November, 1999, when the seasonal variations are weak (compare Figures 3a and 3b). Although gradually recovering, the BoB OHC loss due to the TCs remains about -37×10^{18} J from MR-NoTC and about -30×10^{18} J from RcWIND-NoTC by the end of February, 2000. By examining the purple line (MR-NoTC) in Figure 3b, we obtain that TC1 (10/15–10/19) reduces the OHC by ~70 × 10^{18} J before TC2's (10/25–11/3) emergence, while TC1 + TC2 reduces the OHC by ~145 × 10^{18} J three days after TC2's dissipation. Both TCs are responsible for the negative OHC anomalies in early November.

3.1.2.3. Contribution of TC-Induced OHT to OHC

[19] The BoB OHC loss results from both the NetHF loss and southward OHT anomalies induced by TCs (Figures 3c and 3d). Our results show that the TC-associated winds are the dominant factor that affects the OHT (Figure 3c; compare the green and red with purple and black curves). Of particular interest is that instead of producing a northward OHT anomaly that compensates the NetHF loss, the TCs induce a southward OHT anomaly, which significantly contributes to the OHC loss. This is because the TC-associated winds in the MR alters the currents, which transport the warm ML water southward out of the BoB along the western boundary (not shown). Previous model results have shown that TC-induced vertical mixing leads to DOHP into the thermocline, which can influence transports and energetics of circulation patterns, such as the subtropical cells and gyres [*Jansen et al.*, 2010; *Sriver et al.*, 2010; *Sriver and Huber*, 2010; *Fedorov et al.*, 2010; *Manucharyan et al.*, 2011]. Our results suggest that in the BoB, TC winds can directly influence the wind-driven circulation, leading to increased southward OHT out of the BoB on relatively short (e.g., weeks to months) time scales via changes in the near-surface currents. The implications for longer time-scale background circulation patterns in the BoB remain unclear and require further investigation.

[20] After the TCs pass the BoB, the accumulated (i.e., time-integrated) southward OHT anomaly induced by the TCs start to weaken after mid-November (Figure 3c), consistent with previous studies. However, the TC-induced anomalous OHT does not completely disappear even during February 2000, indicating that the two TCs induce BoB net heat loss. Surprisingly, the reconstructed strong winds (RcWIND) do not have an apparent additional impact on the accumulated OHT, compared to the CCMP winds in the MR throughout the period of interest. The 18-m/s (35-kt) radii of TC1 and TC2 are usually smaller than 220 km (~120 nautical miles), and the effective range of the reconstructed wind only reaches 2 times of the radii (see Table 1 and section 2.1 for space ramping). Given that the TC winds are reconstructed only when the TC centers are located to the north of 14°N, the reconstruction does *not* alter the wind pattern near 10°N (see part 1, Figures 2 and 3). Thus the meridional OHT across 10°N of RcWIND has similar strength and variability as that of the MR.

[21] The effects of TC-associated precipitation and radiation on the accumulated meridional OHT across 10°N are small (MR-NoRAIN and MR-NoRAD; yellow and gray curves in Figure 3c). The weak precipitation effect differs from the *Hu and Meehl* [2009], likely due to the persistently strong stratification in the BoB where strong monsoon precipitation and fresh water input from surrounding rivers make the BoB one of the freshest places in the world's oceans. Consequently, TC-associated precipitation may not alter the stratification much, which may be a unique feature of the BoB, in contrast to *Hu and Meehl* [2009] who examined the Atlantic Ocean.

3.1.2.4. Contribution of TC-Induced NetHF to OHC

[22] The TC-induced accumulated NetHF differences (Figure 3d) represent the impacts of the TC-associated forcing fields on air-sea heat exchange. Post-storm surface fluxes are important, because they contribute to restoring cold wakes caused by TC mixing. Here we use modeled NetHF to estimate the amount of DOHP associated with TC1 and TC2, by examining surface heat flux differences during, and in the months following the TC events. As discussed in part 1, DOHP is defined as the amount of heat mixed irreversibly into the thermocline, thus representing a net oceanic heat convergence. Previous efforts have attempted to quantify DOHP by examining cold wakes using surface observations and assuming they represent homogenized cold anomalies compared to pre-storm conditions, which enables estimation of the amount of heat lost from the upper ocean through vertical mixing [*Sriver and Huber*, 2007; *Sriver et al.*, 2008]. This technique neglects the heat flux to the atmosphere during the TCs, which is suggested to contribute 15 ~ 20% of TC-induced SST reduction [e.g., *Price*, 1981; *Black*, 1983]. Here we estimate DOHP by analyzing post-storm NetHF that act to restore the storm-induced upper-ocean cold anomaly. We directly calculate the accumulated NetHF differences among the model simulations (Table 1) to diagnose the effect of TC-associated forcing fields on ocean surface heat budget. By analyzing the post-storm flux differences between the simulations, rather than comparing post-storm versus pre-storm conditions, we avoid the previous inherent assumptions about the dominance of mixing over surface heat fluxes in cooling the SST. Moreover, it allows us to estimate the significance of post-storm surface fluxes for cold wake restoration for the TCs and conditions under consideration, which has been hypothesized to be important for understanding how TCs impact oceanic heat budgets. The accumulated NetHF difference between RcWIND and NoTC will then represent the best estimate of DOHP effect in this research.

[23] The accumulated NetHF in the BoB from the difference solutions, MR-NoTC and RcWIND-NoTC, have comparable magnitudes to those of OHT (compare Figures 3c and 3d). The TCs induce oceanic heat loss when they pass the

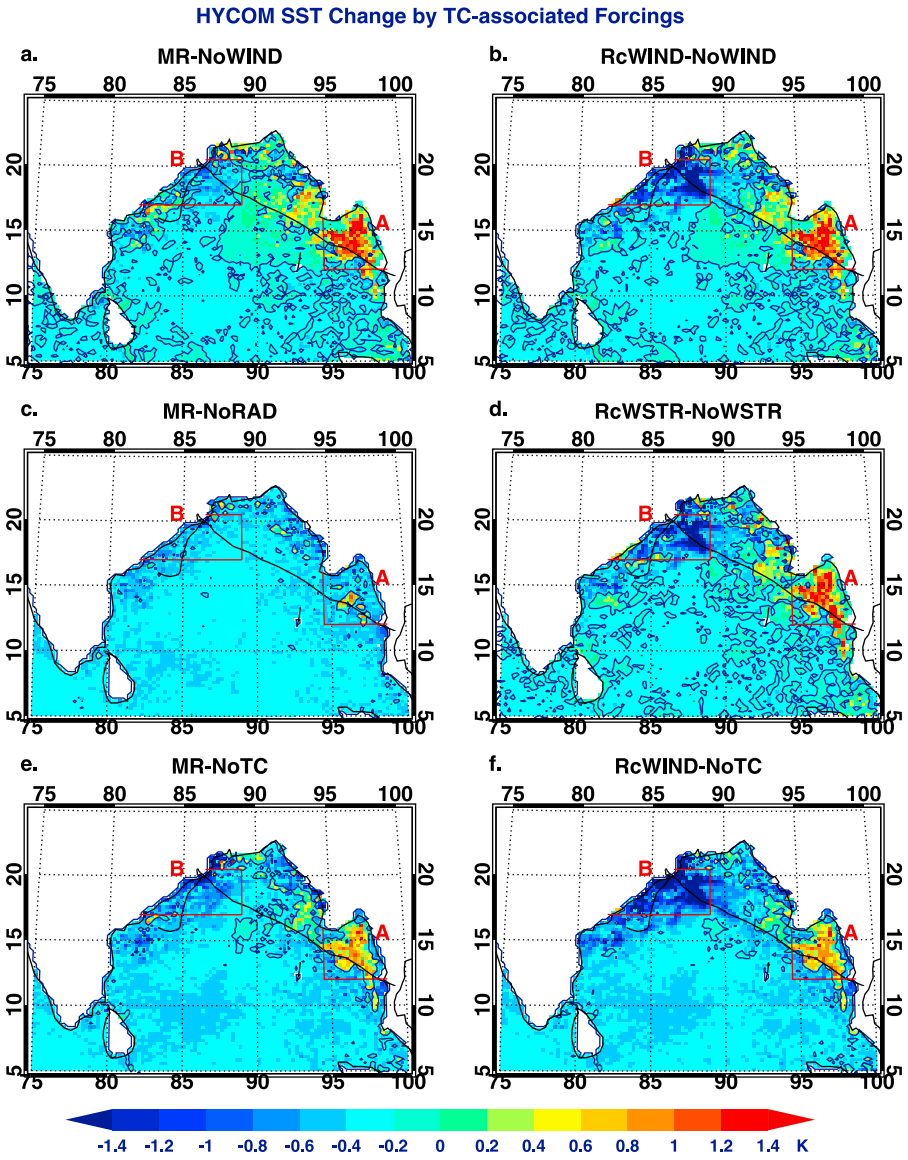

Figure 4. (a) SST difference between the MR and NoWIND for 11/3 mean. (b–f) Similar to Figure 4a, but for the differences between RcWIND and NoWIND, between the MR and NoRAD, between RcWSTR and NoWSTR, between the MR and NoTC, and between RcWIND and NoTC, respectively.

BoB from mid-October to early November, and then cause gradual heat gain in the following few months. By the end of February 2000, the NetHF from RcWIND-NoTC (best estimate of total DOHP effect of TC1 and TC2) is approximately 1.74×10^{18} J into the ocean (Figure 3d, black curve). While the net surface heat gain after the TCs is consistent with the DOHP effect proposed by previous studies, the strong heat loss during the TCs is not negligible in the BoB, which is in contrast to assumptions made in previous studies analyzing surface observations. In solution MR–NoTC (Figure 3d, purple curve) the NetHF is still negative and does not completely recover by February 2000. This evident difference demonstrates that the underestimation of TC-associated winds by the CCMP product in the MR underestimates the DOHP effects, as is clearly shown by solutions RcWIND–NoWIND and MR–NoWIND (Figure 3d, red and green curves). Interestingly, the NetHF loss during the TCs are dominated by the radiative flux forcing, whereas the strong TC winds play an important role in generating the eventual net heat gain near the end of February (compare the black, gray and purple curves in Figure 3d). Convective clouds associated with the TCs reduce the shortwave flux (not shown) and induce the negative NetHF anomaly, cooling the ocean when they pass the BoB. This cooling gradually recovers after the TCs' passage, because the colder SST (Figure 4c) reduces the THF loss. By the end of February, the accumulated NetHF due to radiative flux forcing is approximately -17×10^{18} J.

[24] Compared to the radiative flux, effects of TC-winds on the BoB-averaged NetHF are weak (Figure 3d, green and red curves). In our simulations, wind stress is the major cause for the accumulated THF reduction during the

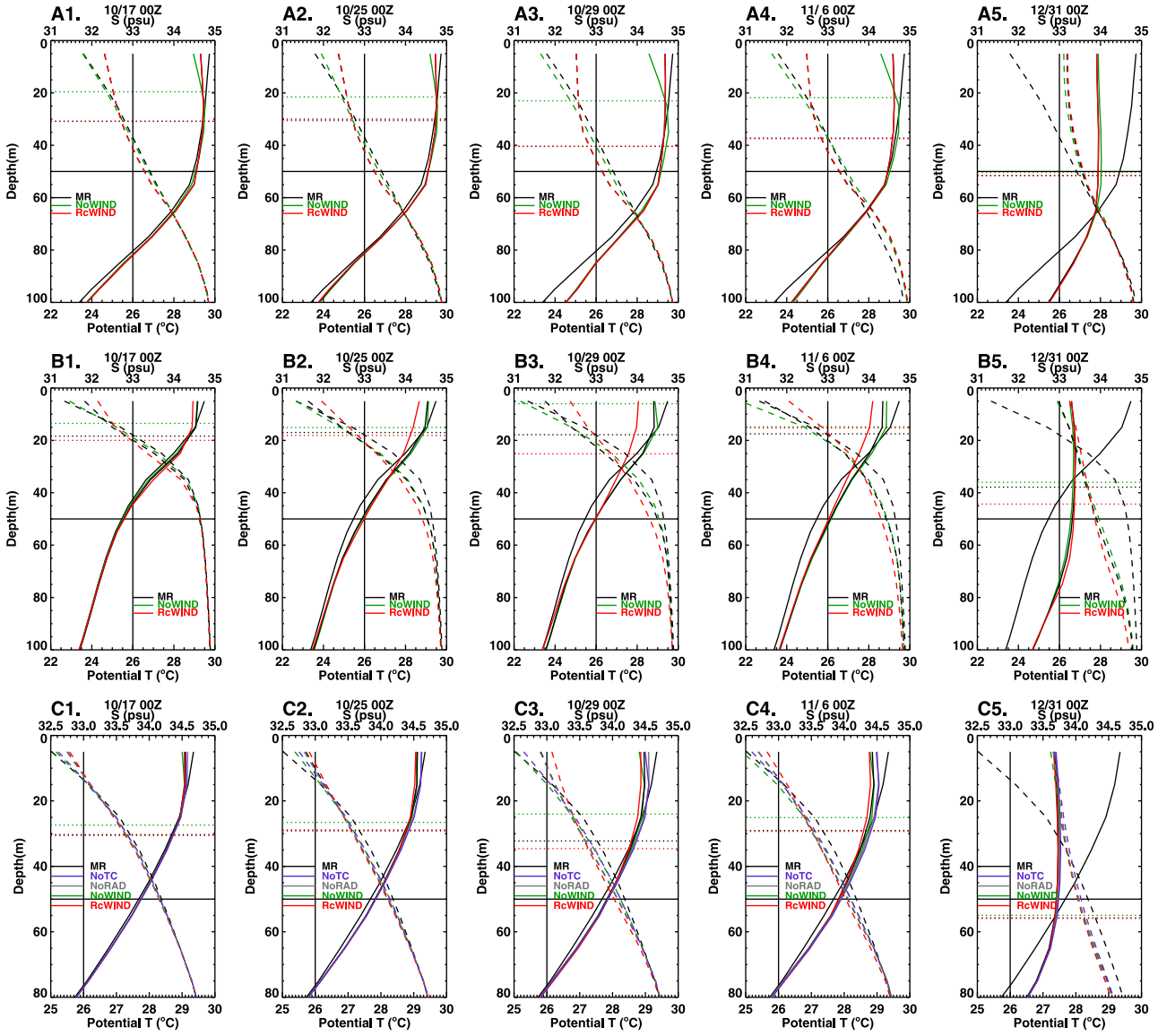

Figure 5. The potential temperature (solid lines) and salinity (dashed lines) profiles during and after TC1 and TC2 (a) for top 100 m of Region A, (b) for the top 100 m of Region B, and (c) for the top 80 m of the BoB to the north of 10°N. The thin black curves are the potential temperature and salinity profiles at 10/11 00Z, four days before TC1, and thus all the model runs share identical potential temperature and salinity profiles according to our experiment design. The dotted lines show the mixed layer depth for the MR (black), NoWIND (green) and RcWIND (red).

recovery after the TCs, with wind speed induced THF being negligible (Figure 3d, compare the green, blue dashed and blue dotted curves). The CCMP wind stress is used in the MR for the entire BoB and in the RcWIND run to the east of 95°E and south of 14°N. The TC-wind stress entrains the warm water below the temperature inversion layer and warms up the SST in the southeastern BoB (see later in this subsection for temperature inversion) in Region A (Figure 4). As a result, THF loss increases in the MR and RcWIND (equations (4) and (5) and Figure 2). When the TCs approach Orissa, strong TC-winds (∼20 m/s in the MR and ∼60 m/s in RcWIND in region B) cool the SST significantly via wind stress, as is seen by the similar SST anomaly patterns and magnitudes in solutions RcWIND–NoWIND and RcWSTR–NoWSTR. The strong wind stress enhances vertical mixing and the cyclonic wind circulation induces upwelling cooling in Region B, resulting in cold SST anomalies. The dominant effects of wind stress and weaker effects of THF due to wind speed on cooling the SST during the TCs' active stages are consistent with previous studies. After the TCs pass the BoB, accumulated NetHF of RcWIND-NoWIND begins to increase because the strong cooling of RcWIND in the northwestern BoB induces a downward THF anomaly, resulting in a net heat gain of $>12 \times 10^{18}$ J at the end of February (Figure 3d, red curve). This effect is counteracted by the warm SST anomaly in the southeastern Bay (Figure 4). These results, combined with the discussion on

Table 2. The TC Effects on Oceanic Heat Convergence (See Text) Using the Method of *Sriver and Huber* [2007] and *Sriver et al.* [2008] and the Data From NCEP, TMI, and HYCOM

Estimate Heat Convergence	TC1	TC2
NCEP SST/50 m mixing depth [*Sriver and Huber*, 2007]	1.18×10^{20} J	7.76×10^{19} J
RcWIND SST/50 m mixing depth	1.03×10^{20} J	1.24×10^{20} J
TMI SST/climatological mixing depth [*Sriver et al.*, 2008]	8.53×10^{19} J	1.18×10^{20} J
RcWIND SST/RcWIND mixing depth	6.86×10^{19} J	1.16×10^{20} J

OHT, demonstrate that TCs indeed have the DOHP effect in the BoB due to both radiative fluxes and strong winds, when the strong TC winds are realistically represented. The pumped heat is transported southward out of the BoB by the oceanic circulation, which itself is enhanced by the TC winds and thus affects the OHT and OHC.

[25] To understand further why the MR-NoTC does not produce the net surface heat gain in February whereas the RcWIND-NoTC run does, we analyze the hierarchy of HYCOM solutions. While the fresh ocean surface favors barrier layer formation [*Lukas and Lindstrom*, 1991; *Sprintall and Tomczak*, 1992] and seasonal surface cooling favors the formation of shallow temperature inversion [e.g., *Shetye et al.*, 1996; *Han et al.* 2001; *Howden and Murtugudde*, 2001; *Masson et al.*, 2002; *Vinayachandran et al.*, 2002; *Sengupta et al.*, 2008] in Region A, which is <25 m (green lines in Figures 5a1–5a4), vertical mixing caused by the CCMP winds in both the MR and RcWIND deepens the ML (Figures 5a1–5a4, red and black lines, and Figure 7) and erodes the temperature inversion. Note that the winds are the same for the MR and RcWIND run in Region A. The deeper ML and mixing with the warm water from below in the MR and RcWIND keep the SST in Region A from decreasing, producing the positive SST anomalies, compared to the NoWIND and NoTC experiments (Figure 4). The warm SST anomalies increase the THF loss, which balances or even exceeds the reduced THF loss associated with TC-induced cold SST in other regions (Figure 4), producing a negative accumulated NetHF in solution for MR-NoWIND and impedes DOHP. The strong stratification and temperature inversions make the BoB a place that has weaker DOHP effects associated with TCs. Nevertheless, our model results suggest TCs can still substantially alter OHT in the BoB region through wind-induced changes in the near-surface circulations.

[26] In contrast, in the northwestern BoB the SST is considerably lower in the RcWIND experiment than the MR. This is because the CCMP winds exceed 20 m/s in Region B for both TC1 and TC2, while the reconstructed winds exceed 45 m/s for TC1 and 65 m/s for TC2. The much stronger winds in RcWIND enhance vertical mixing (see the crossing of the red lines and black lines in Figures 5b1 and 5b2) as well as upwelling (Figures 5b1–5b4), and thus cause much colder SST in a large area in the northwestern Bay. The decreased SST reduces THF loss in the following months, which exceeds the increased THF in region A, producing a positive NetHF anomaly in the BoB and DOHP in the RcWIND run.

[27] As pointed out in section 3.1.2.1, seasonal surface cooling begins in November, when the BoB experiences transition from the summer to winter monsoon. The THF loss is enhanced by the cold and dry air associated with winter monsoon. Meanwhile, the downward solar radiation declines. Therefore, the temperature in the upper 35 m of the BoB dramatically decreases for all the model runs by the end of 1999 (Figures 5a5, 5b5, 5c5, and 3a). After TC2 decreases the BoB SST, the SST actually keeps decreasing in November and December, 1999 and never recovers to its pre-storm value. As a result, one may need to take into account the effect of seasonal cycle, if we quantify the TC effects on DOHP using SST values before and after TCs.

[28] To summarize, sections 3.1.2.3 and 3.1.2.4 show that the strengthened winds and reduced solar radiation due to TC1 and TC2 are the two dominant forcings that change the BoB OHC. While the reduced solar radiation directly decreases the heat input into the ocean, the strengthened winds enhance southward Ekman transport that carries additional OHC out of the domain. Due to the transition from the summer to winter monsoon starting from November, seasonal surface cooling places a cap on the SST recovery from the TCs' impacts through THF.

3.2. Estimated DOHP Based on SST Before/After the TCs

[29] Section 3.1.2.4 shows our estimates of DOHP effect ($\sim 1.74 \times 10^{18}$ J for RcWIND-NoTC in four months) by contrasting the accumulated NetHF from different model runs. In order to better demonstrate the discrepancy between our method and the previous researches, we compute the oceanic heat convergences by TC1 and TC2 based on the methods described in *Sriver and Huber* [2007] and *Sriver et al.* [2008] using the mixing depth and SST from RcWIND and compare with observation-based estimates using the same methodology (Table 2). Specifically, the oceanic heat convergence is defined using the difference between conditions before and after TCs along the wakes, and we also assume a uniform mixing depth of 50 m [*Sriver and Huber*, 2007] and climatological mixing depth [*Sriver et al.*, 2008] for the observation-based estimates.

[30] The SST from RcWIND and NCEP [*Kalnay et al.*, 1996] estimates roughly equivalent oceanic heat convergence, when mixing depth is presumed to be 50 m and footprint is set to $6^\circ \times 6^\circ$ surrounding the TC centers. The oceanic heat convergence estimated by the simulated SST from the RcWIND run is 1.03×10^{20} J for TC1, which is close to the 1.18×10^{20} J estimated from the observed SST as in *Sriver and Huber* [2007]. For TC2, the heat convergence estimated by the simulated SST is 1.24×10^{20} J, which is 60% larger than the estimate of 7.76×10^{19} J based on the observed SST. In *Sriver et al.* [2008], the mixing depth is set to the depth to where the SST change corresponds to the climatological vertical temperature difference. In other words, the mixing depth is the level from which upwelling must occur to achieve a SST response based on the local climatological vertical temperature profiles. In addition, the NCEP SST is replaced by the TMI SST. Using the same concept, we estimate the mixing depth using the RcWIND run and obtain the oceanic heat convergence to be 6.86×10^{19} J for TC1, which decreases by ~33%, and

1.16×10^{20} J for TC2, which reduces by 6.8%. The new mixing depth on average appears to be shallower than 50 m for TC1 in the RcWIND experiment and produces less oceanic heat convergence. These values are comparable to the *Sriver et al.* [2008] estimates of 8.53×10^{19} J and 1.18×10^{20} J for TC1 and TC2, respectively.

[31] Although using the SST and mixing depth from RcWIND would produce the oceanic heat convergence similar to *Sriver and Huber* [2007] and *Sriver et al.* [2008], the estimates of oceanic heat convergence for both TC1 and TC2 are much larger than the accumulated NetHF differences at the end of February, 1999 shown in Figure 3d. This is because a) Sriver et al. assume that the SST reduction after TCs is caused solely by turbulent vertical mixing, and b) in HYCOM the additional NetHF due to lower SST is not sufficient for full SST restoration back to the pre-storm values. As discussed in the previous section, the reduced downward radiative flux during TC1 and TC2 results in significant decrease of NetHF accumulation and thus decrease of SST, and also cancels out most of the increases of NetHF accumulations that result from the TC-induced low SST after the TCs. Furthermore, the SST cooling induced by TC1 and TC2 never fully recovers to the pre-storm values under our scenarios because of the seasonal transition into winter capping the SST restoration. Also note that the role of OHT in SST variations is not clear and needs more investigation.

[32] Our results demonstrate that the assumption of "negligible NetHF influence during the TCs" appears to be invalid for the BoB. Consequently, the estimated DOHP using observed SST before/after the TCs may significantly overestimate the DOHP effects. While the NetHF influence during the TCs may be minor in other ocean basins [e.g., *Price*, 1981; *Black*, 1983], we suggest considering the global DOHP effect estimate based on the methods of *Sriver and Huber* [2007] and *Sriver et al.* [2008] as the upper bound of the actual DOHP effect.

3.3. Penetration of TCs' Impacts in the Upper Ocean

[33] To demonstrate the "penetration" of the TC effects into the ocean, we compare the OHC differences between the MR and EXPs for the upper 10 m, 50 m, 100 m, 200 m and 400 m of the BoB (Figure 6). Note that the 50 m depth is used by *Sriver and Huber* [2007] for estimating the DOHP effects of TCs. In the top 10 m (Figure 6a) within the ML (Figure 5), the ocean immediately feels the radiative flux and THF. The OHC differences between the MR and EXPs are small, and are essentially zero at the end of February 2000, indicating that the TCs' cooling during the TCs can be recovered by the reduced THF loss after TC2.

[34] In the upper 50 m of the BoB, the TC-associated wind and radiative fluxes have comparable influences on the OHC (Figure 6b). The wind has direct impact on the top 50 m OHC via cooling the upper ocean (Figure 5c1–5c5) due to wind-induced mixing and upwelling, which is estimated by the effect of TC-associated wind stress (blue dotted line in Figure 6b). The BoB-averaged ML depth of the MR and EXPs are less than 35 m during the TCs (dotted lines in Figures 5c1–5c5), while the penetration of TC-wind effect in the upper 80 m is clearly shown in the temperature and salinity profiles (solid and dashed lines in Figures 5c1–5c5). The ML and the thermocline layer exchange mass and heat through mixing and entrainment at the ML bottom, which deepens the ML and thins the deeper layer. The OHC exchanges between the ML and the deeper ocean (below ML) can be identified by the opposite signs and comparable magnitudes of the ML OHC anomalies and their deeper OHC anomalies counterparts (not shown). In the top 80 m, vertical mixing induced by wind stress redistributes the OHC vertically.

[35] The CCMP winds in the MR during TC1 (10/15–10/19) and TC2 (10/25–11/3) are stronger than the winds that exclude the TCs in the NoWIND experiment, and hence induce more effective mixing in the upper layer and exchange relatively warmer water in the top 50 m with colder water from below (green line in Figure 6b; see also dashed blue line in Figure 6b for wind stress effect), as well as deepen the ML (Figure 7; green solid line for MR-NoWIND) and induce the heat exchange at the bottom of the ML. According to *Emanuel* [2001], the wind-induced mixing at the bottom of the ML entrains colder water into the ML and at the same time increases the column mass of the ML and warms up the upper thermocline layer. The total column-integrated (surface to bottom) OHC is not changed by TCs if neglecting TC-induced surface heat fluxes, because OHC is only redistributed vertically. However, the strong mixing tends to cool and deepen the ML. We examine this process by observing the negative correlation between the ML depth and ML temperature (Figure 7). The MR, however, has higher ML temperature than NoWIND during TC1 and TC2 due to the formation of temperature inversion in the surface boundary layer in NoWIND. The deeper ML in the MR is caused by the TC-wind induced entrainment, and its warmer ML temperature results from entraining the warmer barrier-layer water from below. In the NoWIND run, winds are weaker, SST is lower and temperature inversion forms. The stronger winds in the RcWIND experiment decrease the top 50 m OHC even more than the CCMP winds in the MR during TC1 and TC2 (Figure 6b, red line for RcWIND-NoWIND) primarily by reducing the upper-ocean temperature further through entrainment and upwelling (compare the red lines with black lines in Figures 5c1–5c3), reaching a peak value of $\sim -52 \times 10^{18}$ J. During TC2, the strong winds in RcWIND also deepen the ML and cool the SST more than the MR (compare red and black dotted lines in Figures 5c1–5c5). The mixing and upwelling signals are induced by wind stress and can be identified by the sudden drops of OHC at the strongest stage of TC1 (10/17 00Z) and TC2 (10/29 00Z) for MR-NoWIND (green), MR-NoWSTR (dashed blue) and RcWIND-NoWIND (red) in Figure 6b for the top 50 m. The reduced OHC gradually recovers. By the end of February 2000, the OHC differences between RcWIND and NoWIND is approximately -3.8×10^{18} J.

[36] The wind effect is also evident in the upper 100 m, 200 m, and 400 m (Figures 6c–6e) during TC1 and TC2. The recovery after the TCs at these depths, however, becomes increasingly slower as depth increases, and the TC-induced OHC change near the end of February becomes increasingly negative. The impacts of TCs on temperature and salinity profiles, however, do not have apparent changes below 80 m (Figure 5), suggesting the importance of TC-induced circulation change on OHT and thus OHC in deeper layers. These results, combined with Figure 3, further demonstrate that the total BoB OHC induced by TCs results from

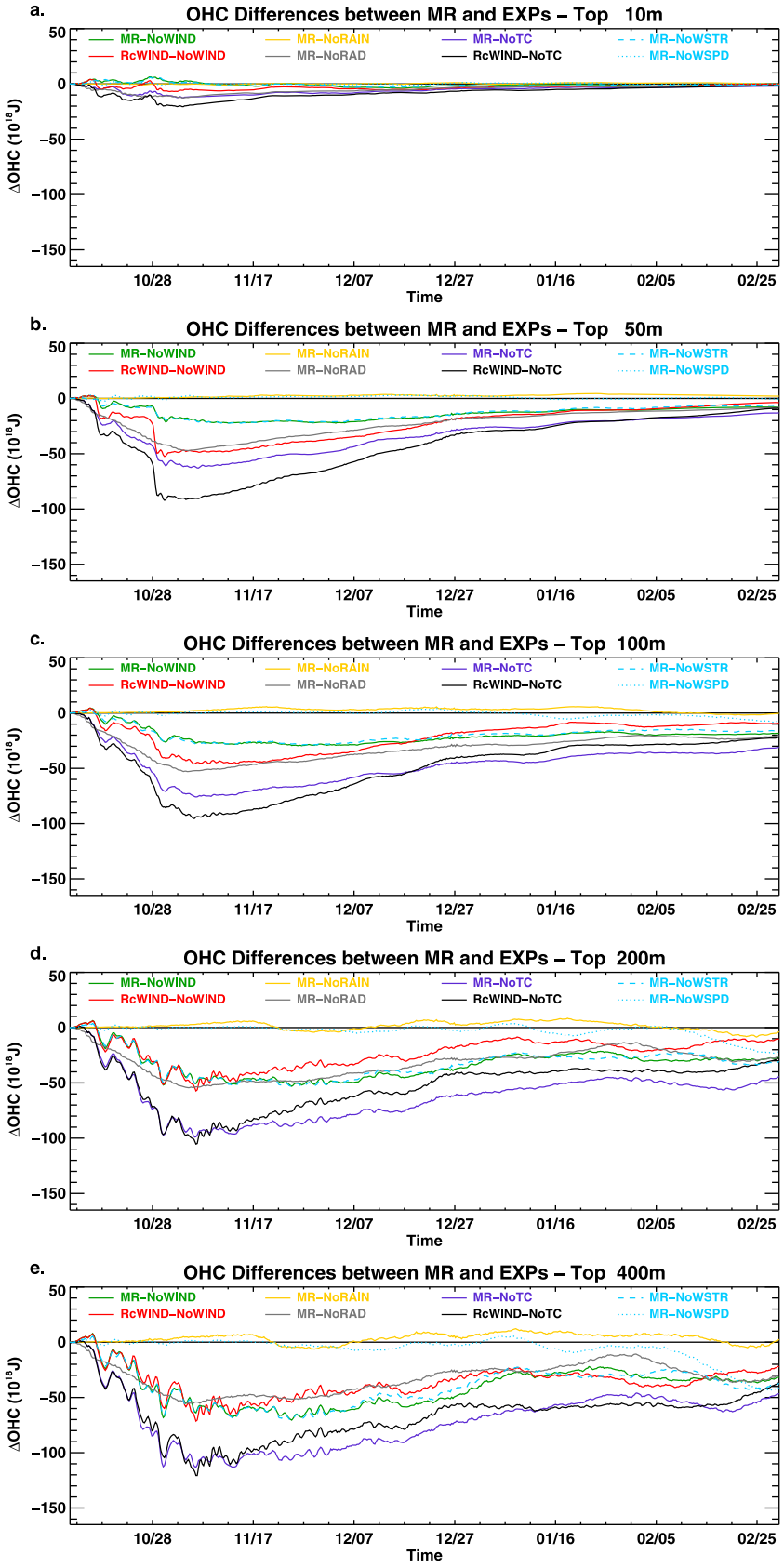

Figure 6. The OHC differences between the MR and a series of EXPs for the to (a) 10 m, (b) 50 m, (c), 100 m, (d) 200 m and (e) 400 m in the BoB (north of 10°N).

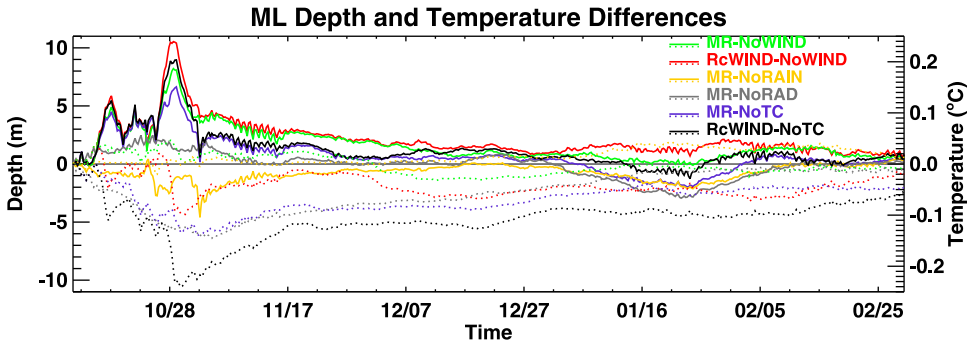

Figure 7. Areal-averaged ML depth (solid) and temperature (dotted) differences between the MR and EXPs.

both the DOHP in the near-surface layer and storm-induced circulation changes, enhancing the southward OHT below the ML. The similarity of the OHC anomalies in the top 200 m and 400 m (Figures 6d and 6e) suggests that impacts of the TCs on OHC via vertical mixing, upwelling and NetHF are mainly confined to the upper 200 m. The TC-induced OHT changes however, can penetrate down to seafloor (not shown) with minor change below 400 m.

[37] Comparing Figure 6e with Figures 3b and 3d, we can see that when considering only wind effect (MR-NoWIND and RcWIND-NoWIND), the TC-induced OHC changes are primarily caused by the anomalous OHT, with wind-induced NetHF playing a minor role. The TC-induced radiative fluxes have comparable effects to winds on the upper-ocean heat content (Figure 6). Although the contribution of the TC-associated radiation to the OHC variations remains identical in the upper 50 m–400 m, the effect of radiative fluxes on the upper OHC varies somewhat with depth. This is because radiative fluxes can affect SST, stratification and therefore mixing and horizontal advection, inducing changes in temperature profile (Figures 6 and 5c1–5c5). The combined effects of the TC-associated wind, radiation and precipitation on the OHC can reach $\sim 114 \times 10^{18}$ J (MR-NoTC) and $\sim 121 \times 10^{18}$ J (RcWIND-NoTC) in the upper 400 m within three days after TC2, and it can reach $\sim 145 \times 10^{18}$ J (MR-NoTC) and $\sim 166 \times 10^{18}$ J (RcWIND-NoTC) for the total column at the same time. Consistent with our above analysis, the TC-associated precipitation has little effect on the OHC in the upper ocean. Note that the temperature of the rain is set to be the same as the SST in HYCOM, and hence the TC-associated precipitation does not directly alter NetHF. This may somewhat underestimate the precipitation effect on SST.

3.4. Impacts of TCs on Ocean Heat Potential

[38] The heat potential is defined as the total OHC above the 26°C isotherm. We are showing heat potential here because it is one of the most important factors for TC development and intensity. The heat potential anomalies can be strongly caused by surface radiative flux differences. The radiation effect (MR-NoRAD) can reach $\sim 20 \times 10^{18}$ J immediately after TC1 and reach $\sim 53 \times 10^{18}$ J immediately after TC2. This amount of heat is similar to the TC-induced accumulated NetHF between the MR and NoRAD at the same time (Figure 3d). They also share similar decaying pattern. This indicates that the BoB heat potential is largely determined by the NetHF in our simulations.

[39] With regard to the wind effect, the BoB heat potential anomalies (Figure 8) are roughly two times of the accumulated NetHF anomalies (Figure 3d) for MR-NoWIND and three times of the accumulated NetHF anomalies for RcWIND–NoWIND immediately after TC2. The behavior of the BoB heat potential change between the three experiments is not similar to the accumulated NetHF in the following four months after TC2. The MR and RcWIND have more surface heat extraction through THF process due to their higher wind speed, compared to the NoWIND run. However, the enhanced THF and thus NetHF process can only partially explain the heat potential response. Vertical mixing is also found *not* to be the main cause for larger heat

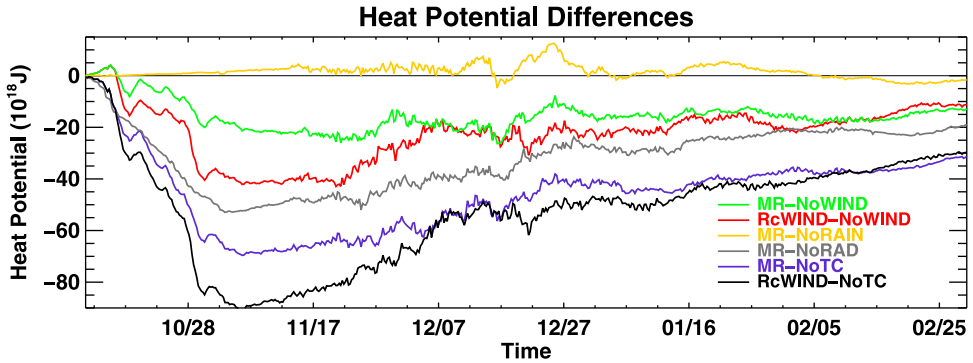

Figure 8. Areal-averaged heat potential of the BoB between the MR and EXPs.

potential response, because the mixing averaged for the BoB generally happened above the 26°C isotherm (Figures 5c1–5c4). The ML depth in the MR averaged for the BoB approximately ranges from 20 m to 35 m before December, 1999, increases to ~56 m by the end of December, 1999, and decreases to less than 40 m by the end of February, 2000. Figure 5 shows that the 26°C isotherm is generally between 75 m and 90 m and only slightly varies among the EXPs. Hence, the vertical redistribution of OHC caused by mixing does not penetrate to the depth of 26°C isotherm, and the BoB heat potential is only slightly altered by vertical mixing. These suggest that the OHT anomalies induced by the TC-associated wind play a major role in changing the BoB heat potential.

4. Summary and Discussion

[40] The two consecutive TCs (TC1 and TC2) significantly reduce the total BoB (north of 10°N) OHC when they pass the BoB, reaching a peak value of -160×10^{18} J in early November after TC2, and the reduced OHC slowly recovers in the following months. The value of OHC change induced by the two TCs is comparable to its seasonal variation from October to mid-November during the monsoon transition period when the seasonal variation is weak, but is only ~10% or less than the OHC seasonal increase during winter monsoon (Figures 3a and 3b).

[41] The reduced BoB OHC during the TCs results from both the southward OHT and reduced downward NetHF anomalies, and both gradually recover in the following months (Figures 3c and 3d). TC winds are the deterministic factor for the OHT change, primarily by causing anomalous ocean circulation that transports heat out of the Bay. The TC-associated surface radiative flux and winds are the two most influential factors that determine the BoB surface NetHF during TC1 and TC2 and in the following months. The reduced radiative fluxes dominate the wind-induced THF during the TCs, due to the TC-associated clouds blocking downward solar radiation. The accumulated radiation effect quickly decays in November right after the TCs, but remains almost constant with a negative anomaly and never returns to zero from December to February 2000. It is the TC-wind effect that causes the recovery of NetHF to a positive value four months after the TCs. The NetHF input into the BoB facilitates the TCs' DOHP effect. Note that only the enhanced reconstructed TC winds are strong enough to produce the DOHP, by causing stronger surface cooling during the TCs through mixing and upwelling processes (Figure 3), and thus stronger recovery after the TCs via increased downward THF. Although the CCMP winds contain TC1 and TC2, the winds are too weak to produce realistic surface cooling. Hence the CCMP wind-induced SST reduction is not enough for enhanced downward THF to compensate for the surface heat loss during the TC events.

[42] The weak upward THF induced by TC winds during the TCs, and the strong wind effect during the recovery after the TCs are consistent with previous studies for the Atlantic Ocean. Different from the Atlantic, our results show large solar radiation effect during the TCs, which compensates for the NetHF recovery after the TCs, producing a weak downward NetHF for a few months after the TCs and making the DOHP effects weak in the BoB. In addition, the effect of TC precipitation has negligible effect of the BoB OHC. These new features are associated with the unique characteristics of the BoB, which is strongly stratified due to monsoon rainfall and large amounts of freshwater input from the BoB rivers. The strong stratification due to fresh waters favors the formation of barrier layer and temperature inversion (Figure 5). As a result, the TC winds entrain warmer water from the barrier layer in the southeastern Bay and thus warm the SST (Figure 4). The warmer SST counteracts the colder SST in the northwestern Bay, causing a weak BoB-averaged downward THF during the recovery period after the TCs.

[43] The weak DOHP effect in the BoB is further investigated by comparing our model results with the estimates of oceanic heat convergence using observed SST based on the existing methods of *Sriver and Huber* [2007] and *Sriver et al.* [2008]. Using these methods (section 3.2), the estimated oceanic heat convergence from both HYCOM SST and observed SST obtain similar magnitudes (Table 2). However, if including the NetHF loss during the TCs, which is neglected by the previous studies, the HYCOM simulated time-integrated NetHF during the recovery period suggests a much weaker DOHP effect in the BoB than the observational estimates. In addition, when considering two consecutive TCs that are less than 6 days apart and the seasonal variations, the BoB temperature structure never recovers to its pre-storm condition between the TCs or after. Because the time between the two TCs is too short for the SST to recover via THF process, the impacts of TC2 on DOHP are not as strong as if TC1 did not exist. The seasonal transition from summer monsoon to winter monsoon immediately after TC2 very likely affects the DOHP estimates based on SST before/after the TCs. By observing climatological seasonal variations of SST in the western Pacific and northwestern Atlantic, which can be as strong as in the northern Indian Ocean, we suspect that the SST recovery in the wakes of TCs in late fall is less than storms occurring earlier in the season due to the seasonal cycle. While this point is important for understanding storm-induced changes in surface budgets, a more robust indicator of DOHP is likely to be the amount of heat mixed irreversible into the seasonal thermocline rather than in cold wake recovery. However, estimating the vertical redistribution of heat through vertical mixing is difficult due to the immediate response in the BoB heat transport and near-surface circulation caused by TC winds.

[44] The effects of TCs can affect both the ML and the deeper ocean below. The entrainment at the bottom of the ML and upwelling induced by the wind stress curl are the primary process for OHC exchange between the ML and deeper ocean and cause mirrored changes in OHC. In the deeper ocean below 200 m, mixing has little influence on OHC, and the TC wind-induced OHT variations dominates the OHC changes, primarily through causing anomalous ocean circulation. The contribution of the OHT to the OHC change is weak below 400 m but keeps accumulating to the bottom of the BoB. The TC-associated rain causes a shallower ML by adding freshwater on top, and therefore the ML temperature changes faster. In contrast, TC-associated radiation deepens the ML because the reduced solar radiation cools the surface and increases mixing. Regarding the BoB

heat potential, TC-associated radiative flux and winds, which drive OHT variations and affect NetHF, are the major causes for the BoB heat potential change (Figure 8).

[45] **Acknowledgments.** We would like to thank Allan Wallcraft for HYCOM consultation, and anonymous reviewers for their constructing comments that helped to improve this manuscript. We also thank CISL of NCAR for providing computer resources and technical support. Jih-Wang Wang and Weiqing Han are supported by NSF CAREER award 0847605, NASA OSTST award NNX08AR62G, and NOAA NA11OAR4310100.

References

Black, P. G. (1983), Ocean temperature changes induced by tropical cyclones, PhD dissertation, 278 pp., Pa. State Univ., State College.

Duchon, C. (1979), Lanczos filtering in one and two dimensions, *J. Appl. Meteorol.*, *18*, 1016–1022, doi:10.1175/1520-0450(1979)018<1016:LFIOAT>2.0.CO;2.

Emanuel, K. (2001), Contribution of tropical cyclones to meridional heat transport by the oceans, *J. Geophys. Res.*, *106*(D14), 14,771–14,781, doi:10.1029/2000JD900641.

Fairall, C. W., E. F. Bradley, J. E. Hare, A. A. Grachev, and J. B. Edson (2003), Bulk parameterization of air-sea fluxes: Updates and verification for the COARE algorithm, *J. Clim.*, *16*, 571–591, doi:10.1175/1520-0442(2003)016<0571:BPOASF>2.0.CO;2.

Fedorov, A. V., C. M. Brierley, and K. Emanuel (2010), Tropical cyclones and permanent El Niño in the early Pliocene epoch, *Nature*, *463*(7284), 1066–1070, doi:10.1038/nature08831.

Gray, M. (1979), Hurricanes: Their formation, structure, and likely role in the tropical circulation, in *Meteorology Over the Tropical Oceans*, edited by D. B. Shaw, pp. 155–218, R. Meteorol. Soc., Bracknell, U. K.

Han, W., J. P. McCreary, and K. E. Kohler (2001), Influence of precipitation minus evaporation and Bay of Bengal rivers on dynamics, thermodynamics, and mixed layer physics in the Indian Ocean, *J. Geophys. Res.*, *106*, 6895–6916, doi:10.1029/2000JC000403.

Howden, S. D., and R. Murtugudde (2001), Effects of river inputs into the Bay of Bengal, *J. Geophys. Res.*, *106*(C9), 19,825–19,843, doi:10.1029/2000JC000656.

Hu, A., and G. A. Meehl (2009), Effect of the Atlantic hurricanes on the oceanic meridional overturning circulation and heat transport, *Geophys. Res. Lett.*, *36*, L03702, doi:10.1029/2008GL036680.

Jacob, S. D., L. K. Shay, A. J. Mariano, and P. G. Black (2000), The 3D oceanic mixed layer response to Hurricane Gilbert, *J. Phys. Oceanogr.*, *30*(6), 1407–1429, doi:10.1175/1520-0485(2000)030<1407:TOMLRT>2.0.CO;2.

Jansen, M. F., and R. Ferrari (2009), Impact of the latitudinal distribution of tropical cyclones on ocean heat transport, *Geophys. Res. Lett.*, *36*, L06604, doi:10.1029/2008GL036796.

Jansen, M. F., R. Ferrari, and T. A. Mooring (2010), Seasonal versus permanent thermocline warming by tropical cyclones, *Geophys. Res. Lett.*, *37*, L03602, doi:10.1029/2009GL041808.

Kalnay, E., et al. (1996), The NMC/NCAR 40-year reanalysis project, *Bull. Am. Meteorol. Soc.*, *77*, 437–471, doi:10.1175/1520-0477(1996)077<0437:TNYRP>2.0.CO;2.

Lee, T., and J. Marotzke (1998), Seasonal cycles of meridional overturning and heat transport of the Indian Ocean, *J. Phys. Oceanogr.*, *28*, 923–943, doi:10.1175/1520-0485(1998)028<0923:SCOMOA>2.0.CO;2.

Lukas, R., and E. Lindstrom (1991), The mixed layer of the western equatorial Pacific Ocean, *J. Geophys.*, *96*, 3343–3357.

Manucharyan, G. E., C. M. Brierley, and A. V. Fedorov (2011), Climate impacts of intermittent upper ocean mixing induced by tropical cyclones, *J. Geophys. Res.*, *116*, C11038, doi:10.1029/2011JC007295.

Masson, S., P. Delecluse, J. P. Boulanger, and C. Menkes (2002), A model study of the seasonal variability and formation mechanisms of the barrier layer in the eastern equatorial Indian Ocean, *J. Geophys. Res.*, *107*(C12), 8017, doi:10.1029/2001JC000832.

Price, J. F. (1981), Upper ocean response to a hurricane, *J. Phys. Oceanogr.*, *11*, 153–175, doi:10.1175/1520-0485(1981)011<0153:UORTAH>2.0.CO;2.

Sengupta, D., B. Goddalehundi, and D. S. Anitha (2008), Cyclone-induced mixing does not cool SST in the post-monsoon north Bay of Bengal, *Atmos. Sci. Lett.*, *9*(1), 1–6, doi:10.1002/asl.162.

Shetye, S. R., A. D. Gouveia, D. Shankar, S. S. C. Shenoi, P. N. Vinayachandran, D. Sundar, G. S. Michael, and G. Nampoothiri (1996), Hydrography and circulation in the western Bay of Bengal during the northeast monsoon, *J. Geophys. Res.*, *101*(C6), 14,011–14,025, doi:10.1029/95JC03307.

Sprintall, J., and M. Tomczak (1992), Evidence of the barrier layer in the surface layer of the tropics, *J. Geophys. Res.*, *97*(C5), 7305–7316, doi:10.1029/92JC00407

Sriver, R. L., and M. Huber (2007), Observational evidence for an ocean heat pump induced by tropical cyclones, *Nature*, *447*, 577–580, doi:10.1038/nature05785.

Sriver, R. L., and M. Huber (2010), Modeled sensitivity of upper thermocline properties to tropical cyclone winds and possible feedbacks on the Hadley circulation, *Geophys. Res. Lett.*, *37*, L08704, doi:10.1029/2010GL042836.

Sriver, R. L., M. Huber, and J. Nusbaumer (2008), Investigating tropical cyclone-climate feedbacks using the TRMM Microwave Imager and the Quick Scatterometer, *Geochem. Geophys. Geosyst.*, *9*, Q09V11, doi:10.1029/2007GC001842.

Sriver, R. L., M. Goes, M. E. Mann, and K. Keller (2010), Climate response to tropical cyclone-induced ocean mixing in an Earth system model of intermediate complexity, *J. Geophys. Res.*, *115*, C10042, doi:10.1029/2010JC006106.

Vinayachandran, P. N., V. S. N. Murty, and V. Ramesh Babu (2002), Observations of barrier layer formation in the Bay of Bengal during summer monsoon, *J. Geophys. Res.*, *107*(C12), 8018, doi:10.1029/2001JC000831.

Wacongne, S., and R. C. Pacanowski (1996), Seasonal heat transport in a primitive equation model of the tropical Indian Ocean, *J. Phys. Oceanogr.*, *26*, 2666–2699, doi:10.1175/1520-0485(1996)026<2666:SHTIAP>2.0.CO;2.

Wang, J.-W., W. Han, and R. L. Sriver (2012), Impact of tropical cyclones on the ocean heat budget in the Bay of Bengal during 1999: 1. Model configuration and evaluation, *J. Geophys. Res.*, *117*, C09020, doi:10.1029/2012JC008372.

Webster, P. J., C. Clark, G. Chirokova, J. Fasullo, W. Han, J. Loschnigg, and K. Sahami (2002), The monsoon as a self-regulating coupled ocean-atmosphere system, in *Meteorology at the Millennium*, edited by R. Pierce, pp. 198–219, Academic, San Diego, Calif., doi:10.1016/S0074-6142(02)80168-1.